Actin polymerization controls the activation of multidrug efflux at fertilization by translocation and fine-scale positioning of ABCB1 on microvilli

Kristen Whalen[a], Adam M. Reitzel[b], and Amro Hamdoun[a]
[a]Marine Biology Research Division, Scripps Institution of Oceanography, La Jolla, CA 92093; [b]Biology Department, Woods Hole Oceanographic Institution, Woods Hole, MA 02543

ABSTRACT **Fertilization changes the structure and function of the cell surface. In sea urchins, these changes include polymerization of cortical actin and a coincident, switch-like increase in the activity of the multidrug efflux transporter ABCB1a. However, it is not clear how cortical reorganization leads to changes in membrane transport physiology. In this study, we used three-dimensional superresolution fluorescence microscopy to resolve the fine-scale movements of the transporter along polymerizing actin filaments, and we show that efflux activity is established after ABCB1a translocates to the tips of the microvilli. Inhibition of actin polymerization or bundle formation prevents tip localization, resulting in the patching of ABCB1a at the cell surface and decreased efflux activity. In contrast, enhanced actin polymerization promotes tip localization. Finally, interference with Rab11, a regulator of apical recycling, inhibits activation of efflux activity in embryos. Together our results show that actin-mediated, short-range traffic and positioning of transporters at the cell surface regulates multidrug efflux activity and highlight the multifaceted roles of microvilli in the spatial distribution of membrane proteins.**

Monitoring Editor
Keith E. Mostov
University of California, San Francisco

Received: Jun 11, 2012
Revised: Jul 17, 2012
Accepted: Jul 24, 2012

INTRODUCTION

Cortical actin regulates membrane physiology. Actin is necessary for traffic and positioning of membrane proteins and acts as a scaffold for membrane protrusions such as microvilli. During development, the assembly and disassembly of actin at the cell surface controls both egg activation and the subsequent progression through embryogenesis. Following fertilization, successive waves of actin-mediated membrane insertion and retrieval lead to changes in membrane physiology. Similar actin-mediated structural changes, resulting in altered membrane function, are seen in many cell types, ranging from metastasizing cancer cells (Polyak and Weinberg, 2009) to neurons (Dillon and Goda, 2005). However, until recently, the fine-scale dynamics of actin-mediated protein traffic have been difficult to characterize, because they occur at spatial scales below those resolved by light microscopy.

In this study, we exploited the dramatic changes in membrane physiology at fertilization of sea urchin embryos to probe the relationship between actin and multidrug/ATP binding cassette (ABC) transporter activity. Twenty-five minutes after fertilization of sea urchin eggs, efflux transport increases 80-fold (Hamdoun *et al.*, 2004), coincident with the assembly and lengthening of microvilli. Moreover, our previous studies indicated that this rapid increase in efflux activity is mediated by multidrug-like ABC transporters and does not require de novo gene expression or translation of maternal mRNA (Hamdoun *et al.*, 2004; Shipp and Hamdoun, 2012), but rather it is mediated by posttranslational mechanisms. Actin has been implicated in activation of transport at fertilization, because inhibitors of F-actin polymerization prevent increases in both multidrug and amino acid transport (Epel, 1972; Hamdoun *et al.*, 2004).

This article was published online ahead of print in MBoC in Press (http://www.molbiolcell.org/cgi/doi/10.1091/mbc.E12-06-0438) on August 1, 2012.

Address correspondence to: Amro Hamdoun (ahamdoun@ucsd.edu).

Abbreviations used: 3D-SIM, structured illumination microscopy; ABC, ATP binding cassette; ANOVA, analysis of variance; Bf-A, brefeldin A; BSA, bovine serum albumin; DMSO, dimethyl sulfoxide; FSW, filtered seawater; HRP, horseradish peroxidase; MDR, multidrug resistance; MDR1, multidrug resistance protein 1; MIP, maximum intensity projection; ML, maximum likelihood; MPBS, Millonig's PBS; NA, numerical aperture; NaFFSW, sodium-free seawater; PBS, phosphate-buffered saline; PF, postfertilization; P-gp, P-glycoprotein; TBST, Tris-buffered saline (50 mM Tris, 150 mM NaCl, pH 7.4) containing 0.05% Tween 20.

In this paper, we show that the translocation of an ABC transporter along actin filaments to the tip of the microvillus is required for activation of efflux at fertilization. Using structured illumination microscopy (3D-SIM) to generate three-dimensional reconstructions of individual actin filaments, we measured the fine-scale movement of the ABC transporter, ABCB1a, along actin filaments following fertilization. Inhibitors of actin polymerization caused the loss of microvillar tip-localized ABCB1a, while enhanced polymerization resulted in the accumulation of ABCB1a in the microvillar membrane and cell cortex. When microvillar bundle and actin rootlet formation were inhibited, ABCB1a localized in patches at the surface, and transporter activity decreased. In addition, we determined that the Rab GTPase, Rab11, contributes to the activation of efflux activity at fertilization. Until now, relatively little was known about how fine-scale (i.e., nanometer-sized) changes in membrane protein location at the cell surface influence protein function. Our findings point to the importance of short-range traffic in regulation of cell function and have implications for understanding changes in physiological state in a variety of processes, including embryonic development and multidrug resistance (MDR) in cancer.

RESULTS

Sea urchin ABCB1a is a homologue of mammalian ABCB1/MDR1/P-gp

Our previous studies indicated there is an increase in several MDR-like efflux transport activities, including a PSC833-sensitive, that is, P-glycoprotein (P-gp), activity following fertilization of *Strongylocentrotus purpuratus* eggs (Hamdoun *et al.*, 2004). Phylogenetic analysis of sea urchin ABCB proteins with both protostome and deuterostome representatives indicates *S. purpuratus* ABCB1a is a homologue of human P-gp (ABCB1/MDR1; Figure 1A). Consistent with this hypothesis, overexpression of sea urchin ABCB1a reduces intracellular accumulation of canonical substrates such as calcein (Hamdoun, 2009).

Because the increase in multidrug efflux after fertilization does not require expression or translation of ABCB1a mRNA (Hamdoun *et al.*, 2004), we examined whether glycosylation of immature protein could be an alternative mechanism for ABCB1a activation. Overexpression of recombinant ABCB1a in the presence or absence of brefeldin A (Bf-A), an inhibitor of protein transport to the Golgi, or cyclosporin A, an agonist of glycosylation (Loo and Clarke, 1997), revealed that the core molecular weight of ABCB1a is 150 kDa, whereas the mature protein is 185 kDa, similar to the glycoform profile of human P-gp (Supplemental Figure S1). Western blots of endogenous ABCB1a revealed that neither the abundance nor the major glycoform profile change at fertilization (Figure 1B), indicating that mature ABCB1a stored in the egg mediates the postfertilization (PF) increase in activity.

Extension and retraction of F-actin is coincident with activation of transport

In the unfertilized sea urchin egg (~80-µm diameter), a discrete 1-µm-thick "cortex" located just below the plasma membrane contains roughly 10–30% of the total actin (Spudich and Spudich, 1979; Spudich *et al.*, 1988; Otto *et al.*, 1980; Vacquier, 1981). A fraction of this actin is organized into short, F-actin microfilaments (Schroeder, 1979), while the remainder is located immediately subjacent, forming an interconnecting network of microfilaments along the underside of the plasma membrane (Bonder *et al.*, 1989). Following fertilization, cytoplasmic alkalinization triggers the polymerization of actin, leading to the projection of microvilli (Begg *et al.*, 1982), as

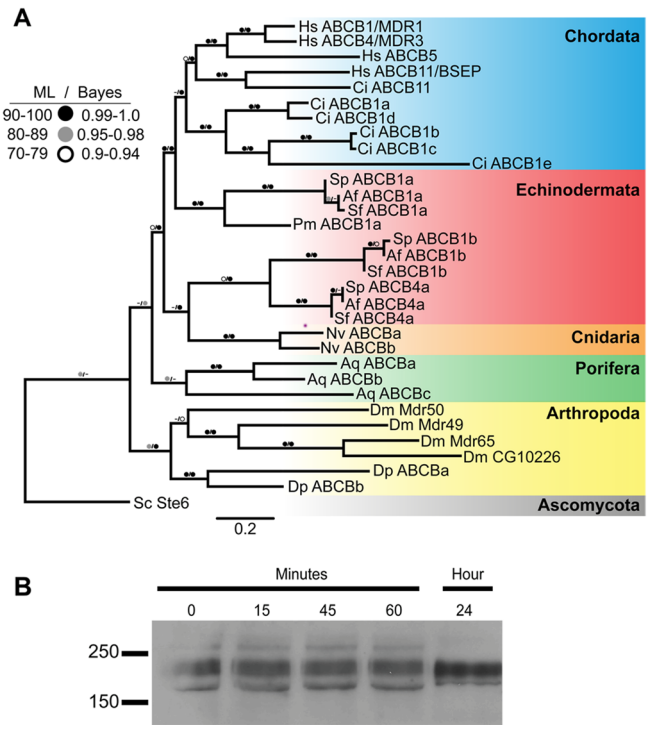

FIGURE 1: *S. purpuratus* (Sp) ABCB1a is a homologue of human P-gp and is present in its mature form in the unfertilized egg prior to activation at fertilization. (A) Phylogenetic relationships of Sp ABCB family transporters with human (Hs), *Ciona intestinalis* (Ci), *Strongylocentrotus franciscanus* (Sf), *Allocentrotus fragilis* (Af), *Patiria miniata* (Pm), *Drosophila melanogaster* (Dm), *Nematostella vectensis* (Nv), *Daphnia pulex* (Dp), *Amphimedon queenslandica* (Aq), and *Saccharomyces cerevisiae* (Sc). (B) Immunoblot of ABCB1a in sea urchin egg and embryo cell lysates probed with Ab1-C1 shows that ABCB1a does not increase in abundance or change in glycoform profile at fertilization.

well as the extension, and then retraction, of actin rootlets into the fertilized egg.

Using confocal microscopy, we characterized changes in F-actin polymerization and ABCB1a localization at fertilization. We found that eggs have short (371 nm), hexagonally arrayed microvilli, composed of F-actin with few or no cortical extensions (Figure 2). Microvilli grew 10-fold following fertilization to a maximum of 3.71 µm at 45 min PF, and then receded slightly to an average length of 2.95 µm at 60 min PF (Figure 2B). In contrast, cytoplasmic actin filaments peaked in length at 15 min PF, extending 5.62 µm into the cytoplasm, then receding to 1.90 µm by 60 min PF (Figure 2B).

Coincident with these actin dynamics, ABCB1a showed pronounced changes in distribution, moving from large patches subjacent to the membrane in unfertilized eggs to discrete spots at the surface of the embryo. Prior to fertilization, 60% of ABCB1a was located in large subcortical patches, interspersed among the negatively staining cortical granules and below the short microvilli (Figures 2A, 3, A and E, and S2). At 15 min PF, these transporter pools started to disperse (Figure 2A); however, > 70% of the transporter was still located at or below the base of the microvilli (Figure 3, B and F). After the increase in activity (45 min PF), 96.5% of the transporter relocated to the base of the microvilli and into the microvillar membrane, with 28% of the total ABCB1a protein located within 1 µm of the tip (Figure 3, C and G). By 60 min PF, a bimodal distribution of ABCB1a was apparent, with 53% of the transporter

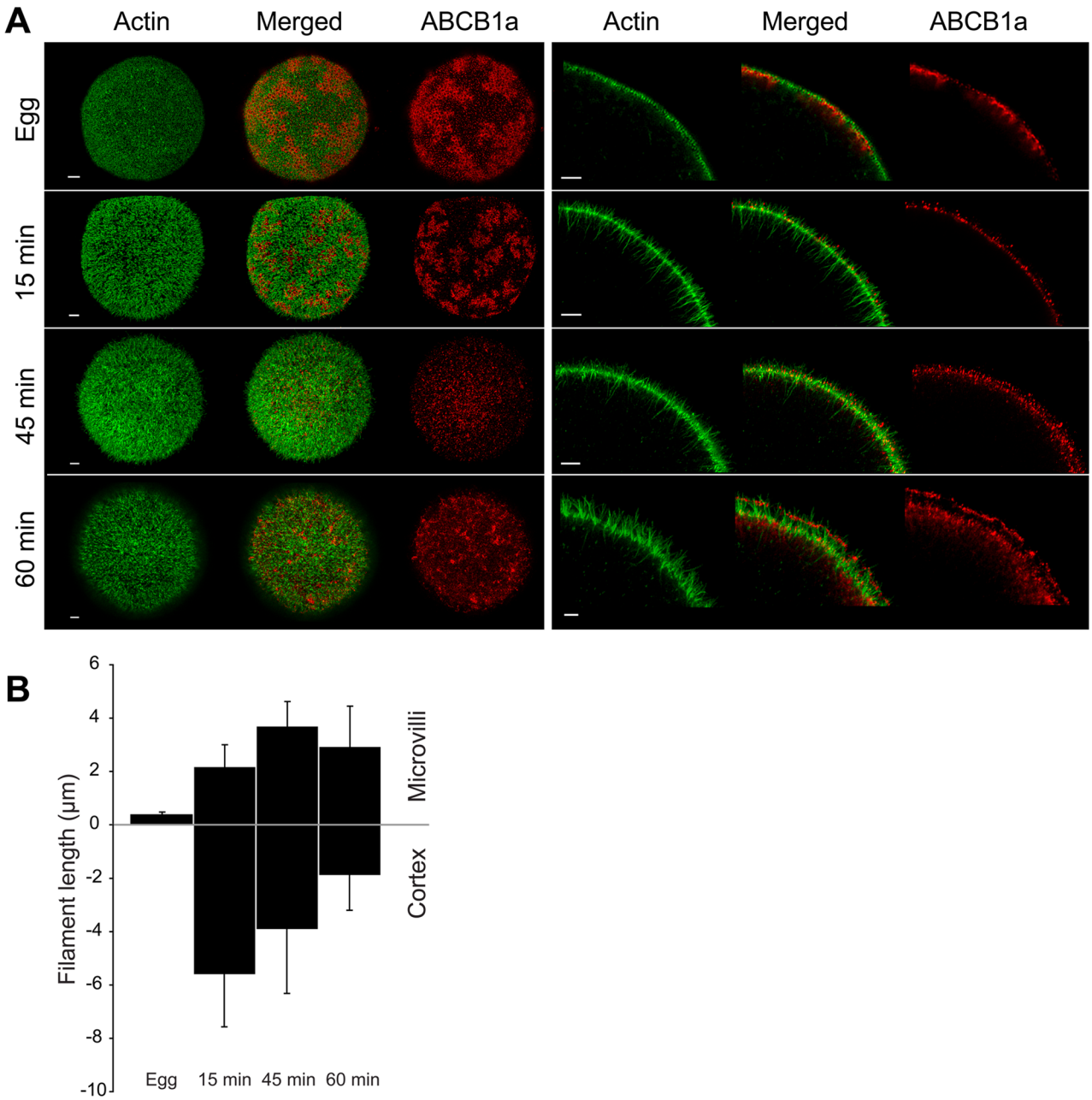

FIGURE 2: Characterization of actin filament elongation and ABCB1a translocation after fertilization, using confocal microscopy. (A) F-actin (green) and ABCB1a (red) in eggs and embryos. Left, MIP; right, cross-sections. Scale bars: 5 and 3 µm, respectively. (B) Bars represent mean length (± SD) of F-actin filaments ($n = 3$ eggs or embryos × 10 filaments per time) extending into the cortex and of microvillar projections. Zero (y-axis) denotes the base of the microvilli.

located on the microvilli, of which approximately 33% had accumulated within 1 µm of the tip (Figures 3, D and H, and S3). The tip localization seen in 60 min PF embryos is maintained in later development, including the 32-cell stage (8 h PF; Figure S4).

Activation of ABCB1a is mediated by short-range translocation along actin filaments

While confocal microscopy reveals the two-dimensional patterns of protein translocation at fertilization, we found the resolution in the axial (or z-dimension) insufficient to determine the precise relationship between transporter spots associated with individual actin filaments. To quantitatively assess the translocation of ABCB1a along F-actin filaments, we used 3D-SIM to create three-dimensional surface reconstructions of individual F-actin filaments and measure the axial location of actin-associated (i.e., transporter spots ≤200 nm from a filament) ABCB1a (Figure S5).

In the unfertilized egg, ~22% of F-actin-associated ABCB1a was within the upper third of the microvillus, that is, 100 nm from the tip (Figure 4A and Supplemental Movie S1). By 15 min PF, the actin filaments associated with the microvilli had grown to an average of 2.19 µm, and 15% of actin-associated ABCB1a was within 750 nm of the tip (Figure 4B and Supplemental Movie S2). In contrast, the

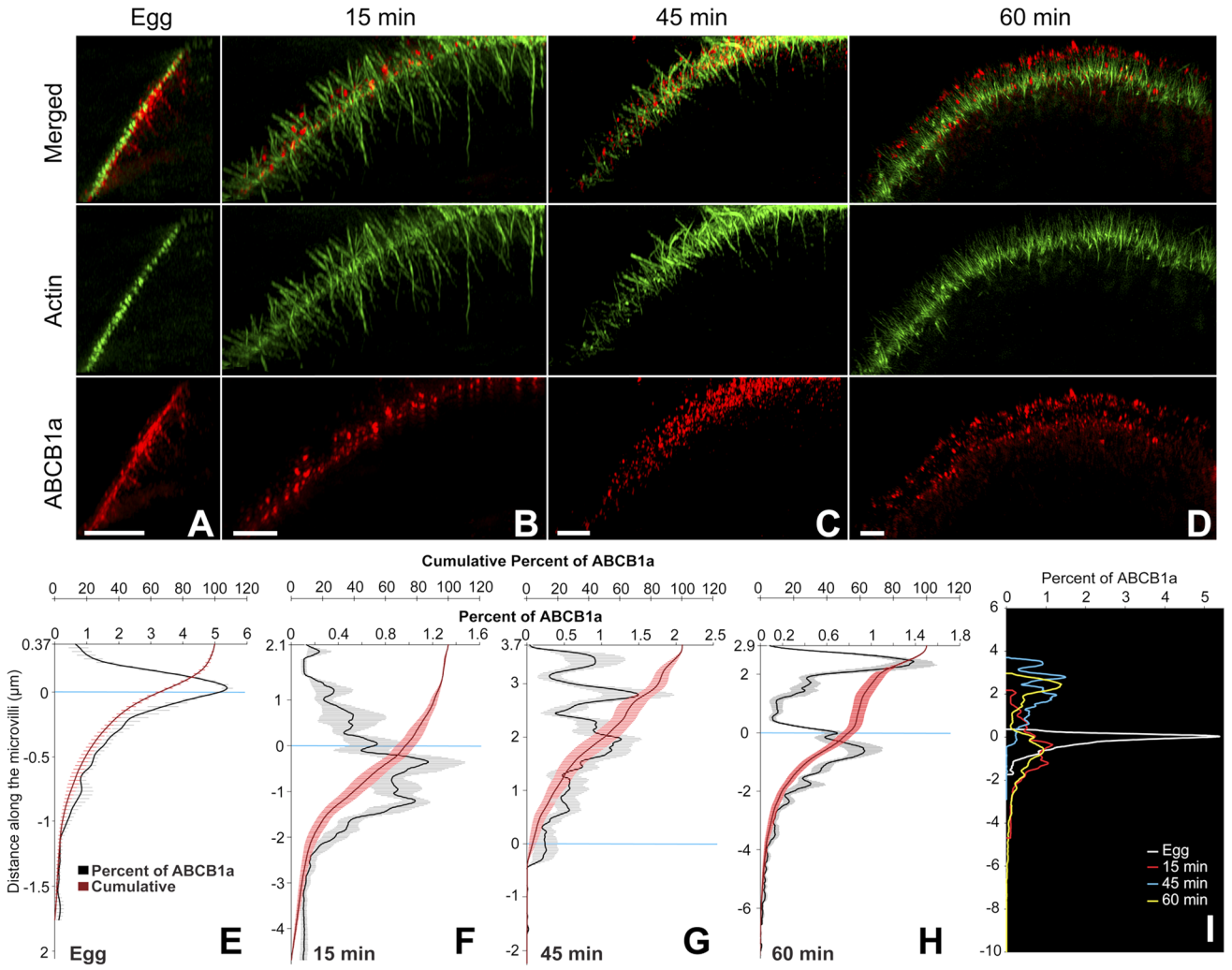

FIGURE 3: ABCB1a translocates to the microvillar tips and has a bimodal distribution at 60 min PF, as visualized by 3D-SIM. Cross-sections of an egg (A) and embryos (B–D) show the localization of ABCB1a in relation to actin filaments. Scale bar: 3 μm. ABCB1a distribution shown as mean percent of total (± SE; black line) and cumulative percent of total (± SE; red line) along an actin filament, as represented by an intensity profile in the egg (E) and embryos (F–H). (I) A summary of the change in ABCB1a distribution over time shown as mean percent of total for egg at 15, 45, and 60 min PF. Zero (*y*-axis) indicates the base of the microvilli.

accumulation of ABCB1a at or near the tip increased to 47 and 49% by 45 and 60 min PF, respectively (Figure 4, C and D; Supplemental Movies S3 and S4), coincident with the increase in efflux activity. In addition, at 60 min PF, embryos no longer had a secondary "pool" of actin-associated transporters at the base of the microvilli extending into the cortex, indicating that the transporter (compared with Figure 3H) is not associated with F-actin and was instead in the cytoplasm.

Actin polymerization and bundle formation is required for tip localization of ABCB1a

Next we investigated how three types of modifications to the actin polymerization state affected ABCB1a localization. First, we examined how actin polymerization inhibitors cytochalasin D and latrunculin A, which are known to perturb efflux activity (Hamdoun *et al.*, 2004), alter transporter location. Both compounds caused the loss of tip-localized ABCB1a and homogenous staining of the cortex, consistent with a role for actin in recruitment of ABCB1a to the cell surface (Figure 5A).

Second, we examined how the loss of actin bundle and rootlet formation in microvilli changed ABCB1a localization and activity in ionophore-activated eggs grown in sodium-free seawater (NaFFSW). Microvilli in these embryos were elongated, but flaccid (Figure 5B), and contained an irregular network of actin filaments, rather than the parallel bundles of normal, erect microvilli (Begg *et al.*, 1982). Immunolocalization of ABCB1a in these embryos revealed significant patching of the transporter in the plasma membrane and cortex and loss of the bimodal distribution and tip localization of ABCB1a seen in 60 min PF controls (Figure 3, D and H). Moreover, the loss of bundled actin resulted in a 1.8-fold decrease in efflux activity (Figure 5B). Together these results confirm that actin architecture and bundle formation are crucial for maintaining transporter activity and localization.

Finally, we examined the effects of jasplakinolide, an actin-stabilizing compound, on recruitment and accumulation of ABCB1a. Consistent with a role of F-actin in promoting tip localization of ABCB1a, jasplakinolide further increased the amount of the protein on microvillar tips (Figures 5A, S6, and S7). Furthermore, because

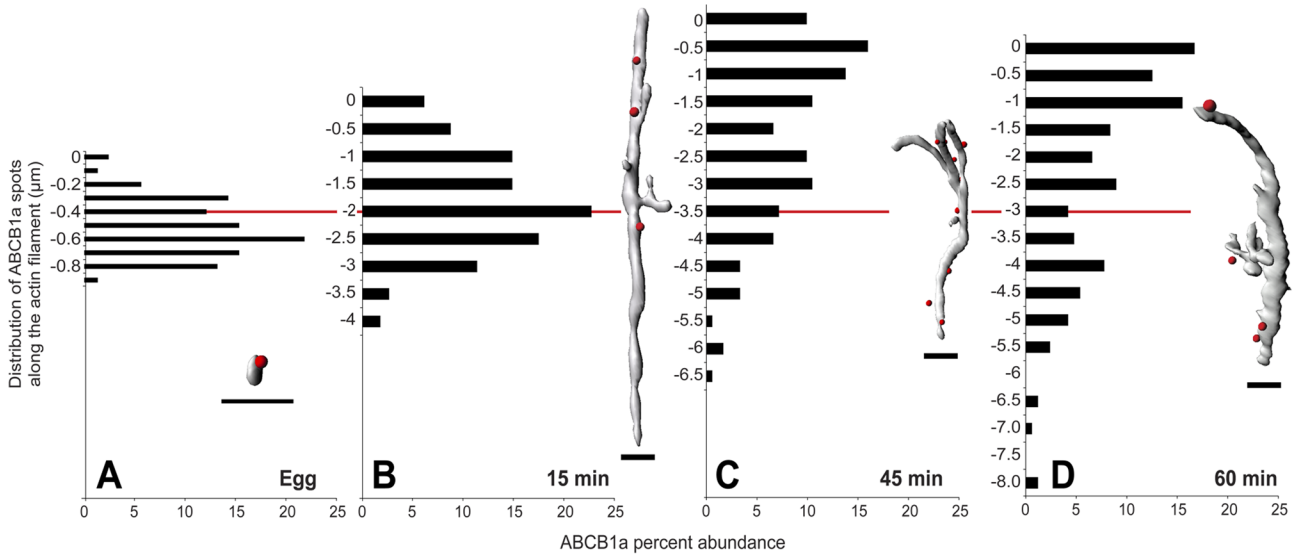

FIGURE 4: Three-dimensional analysis of ABCB1a dispersal relative to F-actin filaments indicates efflux activation is mediated by short-range, actin-dependent translocation. F-actin–associated ABCB1a advances tip-ward after fertilization (A–D). Bars indicate percent of ABCB1a spots within 200 nm of actin surface, and zero (*y*-axis) indicates the tip of the microvillus ($n = 6$ eggs or embryos $\times$ 10 filaments per time). Red line indicates the average microvillar length at each time. Insets, representative actin filament isosurfaces and associated ABCB1a spots (red). Scale bar: 1 µm.

jasplakinolide inhibits the continuous retrograde translocation of actin filaments from the tips to the cell interior, these results also indicate that downward motion of the treadmilling core bundle may be necessary for removal of ABCB1a from the ends of the microvilli. Collectively, these actin perturbation experiments confirmed that F-actin is necessary for the establishment of tip-localized ABCB1a.

Rab11 is required for activation of MDR activity

Previous studies in hepatocytes and cancer cells indicated Rab GTPase cycling is involved in the apical trafficking and endosomal cycling of ABC transporters (Fu and Arias, 2012). Additionally, Rab GTPases have been shown to be enriched in the cortex of sea urchin embryos and function in cortical granule exocytosis after fertilization (Conner and Wessel, 1998, 2000). In light of these observations, we hypothesized that Rab GTPases could also control actin-mediated translocation of ABCB1a to the plasma membrane. Therefore, we conducted a screen of Rab GTPases, interfering with their function by peptide competition with their effector domains, evolutionarily conserved regions specific to each Rab. Unfertilized eggs were injected with dominant-negative Rab effector peptides against Rab4, -5, -7, and -11, and efflux activity was measured after fertilization. While effector peptides designed against Rab4, -5, and -7 had no effect on transporter activity, Rab11 peptides caused a dose-dependent increase in intracellular calcein accumulation, indicating inhibition of ABC transport (Figure 6A). At a Rab11 effector peptide concentration of 200 µM, embryos accumulated 200% more calcein than noninjected, two-cell control embryos (Figure 6B), indicating that Rab11 is necessary for activation of transport.

Rab11 colocalizes with ABCB1a in eggs

In light of the observation that Rab11 effector peptides reduce up-regulation of MDR-like efflux transport, we examined the colocalization of Rab11 and ABCB1a following fertilization using confocal microscopy. Immunolabeling showed that both Rab11 and ABCB1a colocalize to the same patches subjacent to the membrane in unfertilized eggs (Figure 7). By 15 min PF, these Rab11/ABCB1a-containing patches began to disperse, and we saw both Rab11 and ABCB1a insert into the membrane. However, by 60 min PF, ABCB1a moved to the tips of the microvilli, while Rab11 primarily remained in a discrete band at the base of the microvilli (Figure 7), suggesting that Rab11 may assist in the insertion of ABCB1a into the membrane rather than shuttling the transporter to and from the tips.

DISCUSSION

In this study, we show that short-range traffic and precise positioning of transporters at the cell surface is required for complete activation of multidrug efflux after fertilization. Using superresolution microscopy to resolve movements of ABC transporters, we found that activation of ABCB1a in sea urchin eggs involves both actin-mediated recruitment of subsurface stores of the transporter, presumably stored in Rab11-positive endosomes within the egg, and the subsequent translocation of the protein to the tips of microvilli. The total distance the transporter moves in the switch between its *inactive* state in the egg to its *active* state in the embryo is relatively short, on the order of 2–4 µm, or < 5% of the diameter of the egg. Indeed, even at 60 min PF, by which time transport is activated, subcortical "pools" of protein remain within a few micrometers of the surface. These results demonstrate how relatively short-range movements of multidrug transporters at the surface can result in large changes in efflux activity.

These results have implications for understanding the regulation of membrane physiology in both embryonic and adult cells. It has long been known that the polymerization state and density of cortical actin filaments change dramatically in early development, but the functional significance of these dynamics remains unclear. Given our findings and the observation that several other types of actin-dependent membrane transporters are up-regulated after fertilization of sea urchin eggs (Epel, 1972, 1975), we propose that one key role of actin dynamics in early embryogenesis is the control of membrane physiology. Extension of actin rootlets into the cortex could

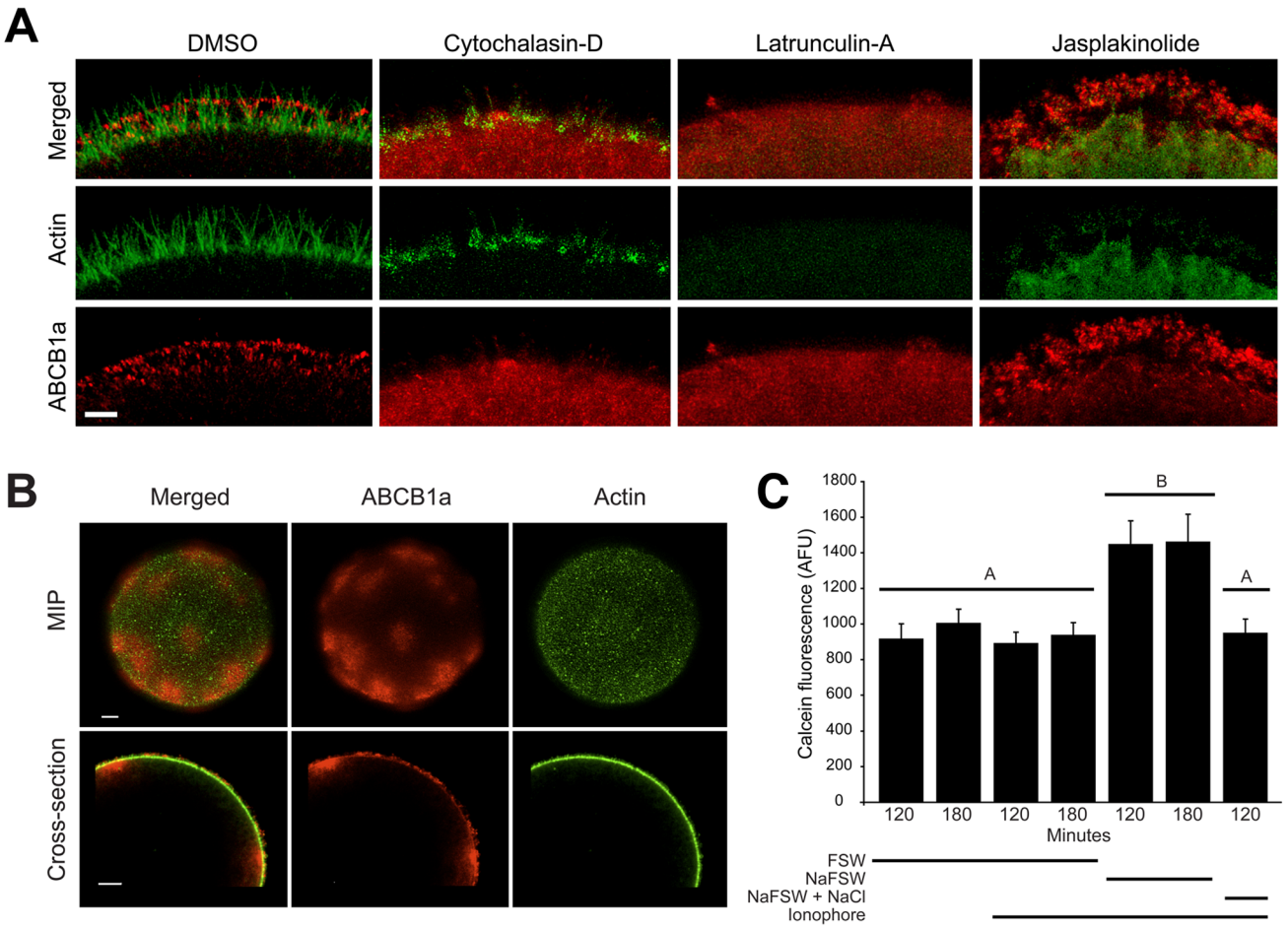

FIGURE 5: Perturbation of actin polymerization and F-actin bundle formation disrupts ABCB1a translocation and causes partial loss of transporter-mediated calcein efflux. Embryos treated with 2 μM jasplakinolide, cytochalasin D, latrunculin A, and DMSO (control) at 10 min PF and imaged at 60 min PF. (A) Cytochalasin D and latrunculin A eliminate ABCB1a accumulation in the cortex, while jasplakinolide increases accumulation of ABCB1a on microvilli. Scale bar: 2 μm. (B) Embryos (MIPs and cross-sections) activated in A23187 and grown in NaFFSW until 60 min PF were stained for actin and ABCB1a. Scale bar: 8 μm. (C) Average (± SE) intracellular calcein fluorescence (120 and 180 min PF) activated with A23187 and cultured in either NaFFSW or NaFFSW+NaCl ($n = 10$ embryos × 10 batches). A significant increase in calcein accumulation was observed in A23187-activated embryos cultured in NaFFSW (1.8-fold) at both 120 and 180 min PF. Letters denote significance (analysis of variance [ANOVA], $p < 0.001$).

be necessary for recruitment of subsurface stores of membrane proteins and trafficking machinery, while actin projections (i.e., microvilli) could facilitate their optimal positioning at the surface. Consistent with this hypothesis, we recently observed that efflux activity is down-regulated in micromeres and small micromeres (Campanale and Hamdoun, 2012), which have fewer microvilli than other cells in the embryo (Schroeder, 1988).

Events similar to the actin-mediated translocation of ABCB1a described here are likely to be broadly relevant to many cell types. Previous work in epithelial cells suggests that actin-mediated surface cycling of ABC transporters is necessary for control of their surface concentration and activity (Guggino and Stanton, 2006; Fu and Roufogalis, 2007) and that disruption of this process can lead to disease. For example, the loss of apical targeting of ABCB4/B11 in hepatocytes results in cholestasis (Wang *et al.*, 2002; Nicolaou *et al.*, 2011), while diminished ABCC7 (cystic fibrosis transmembrane conductance regulator) leads to cystic fibrosis (Loo and Clarke, 2008). Similarly, acquisition of drug resistance after metastasis of cancer cells requires both increases in the plasma membrane concentration of ABCB1/P-gp (Callaghan *et al.*, 2008) and changes in cortical actin organization (Polyak and Weinberg, 2009). Moreover, it seems that at least some of the cellular machinery that controls the surface titer of multidrug transporters is conserved. For example, we observed that inhibition of Rab11 interferes with up-regulation of transport at fertilization, which is similar to what has been observed in polarized WIF-B9 cells, in which Rab11, via its interaction with myosin Vb, was shown to be necessary for actin-mediated surface expression of apical ABC transporters (Wakabayashi *et al.*, 2005). One caveat of our results was that Rab11 effector peptides did not completely block up-regulation of transport activity; that is, they did not restore accumulation levels to those observed in the unfertilized egg. However, since our previous studies (Hamdoun *et al.*, 2004) demonstrated that there are multiple efflux transporters in eggs, a likely explanation is that the activation of these other transporters, such as ABCC1/MRP, is not mediated by Rab11.

Another question raised by the effector peptide results was whether Rab11 could activate transporters indirectly, for instance, by trafficking an activating kinase (Shi *et al.*, 2009). We observed

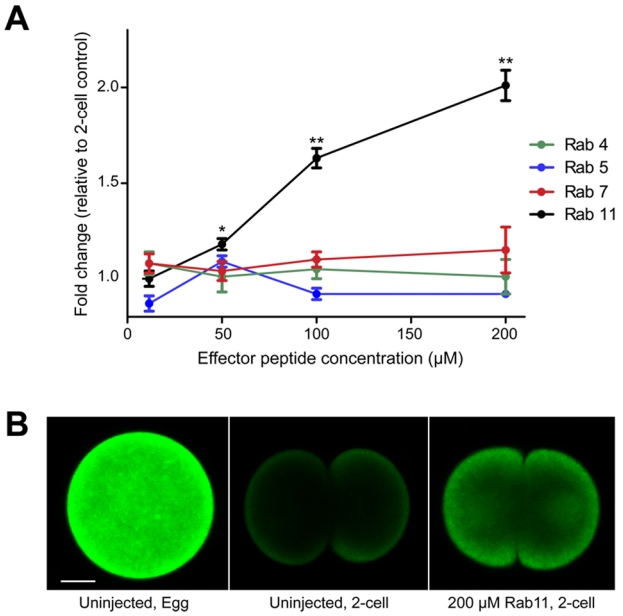

FIGURE 6: Rab11 is required for activation of MDR activity. (A) Fold change in calcein fluorescence in Rab effector peptide–injected embryos relative to a two-cell control embryo. The average calcein fluorescence of 20 embryos (± SEM) is shown. Asterisks indicate significant differences from a two-cell control embryo (ANOVA, *, $p = 0.0016$, **$p < 0.0001$). (B) Representative egg and two-cell embryos (150 min PF) showing differences in calcein accumulation after injection with 200 μM Rab11 effector peptide.

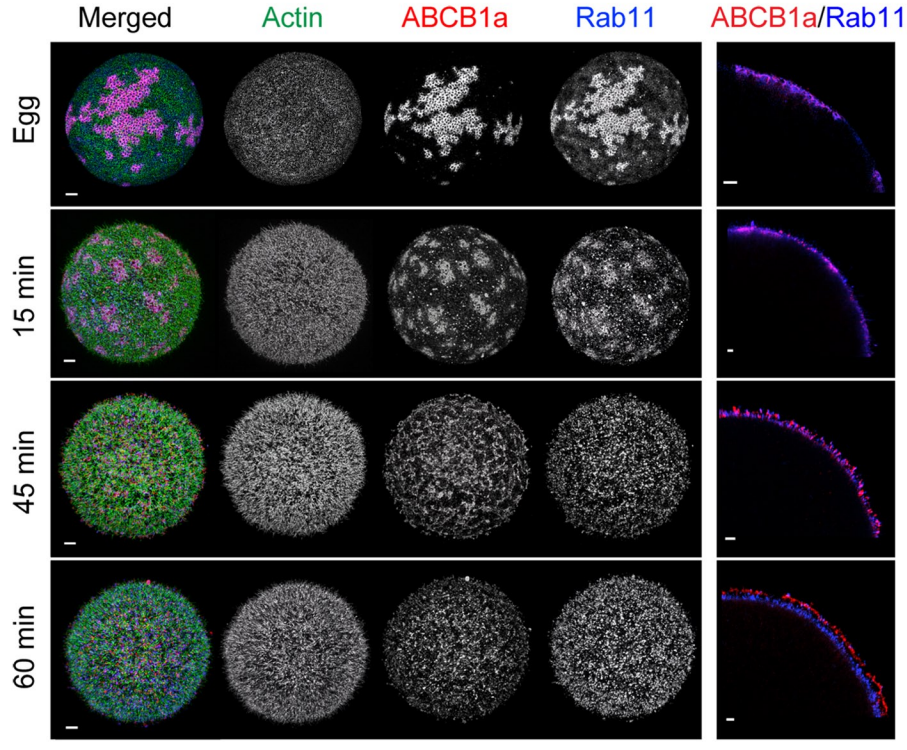

FIGURE 7: Rab11 colocalizes with ABCB1a in unfertilized eggs. MIP (four left panels) and cross-sections (right-most panels) of an egg and embryos depict the localization of Rab11 in relation to ABCB1a and actin. Scale bars: 5 and 2 μm, respectively.

that Rab11 effector peptides do not block cell division, unlike what was reported for Rab3 effector peptides (Conner and Wessel, 1998, 2000), suggesting the Rab11 effects are not mediated by interference with major signaling proteins. Furthermore, the close colocalization of Rab11 and ABCB1 in eggs (Figure 7) suggests that the role of Rab11 in transporter activation is more direct. Because myosin is a well-known effector of Rab11, and this motor is necessary for activation of ABCB1 in other cells, it seems most plausible that Rab11 controls the delivery of transporter-containing vesicles to the membrane. Interestingly, we observed that Rab11 does not accumulate at tips of microvilli (Figure 7), further indicating its role may center around the insertion of the transporter into the membrane rather than traffic along the microvillus.

An unexpected finding of this study was the polarization of ABCB1a to the tips of the microvilli, rather than their random distribution along the cell surface. Our results with ionophore (Figure 5) indicated that the bundled architecture of the actin filament, and not simply the microvillar membrane itself, is required for the recruitment/maintenance of tip localization and functioning of ABCB1a. We found that the loss of the actin filament bundle leads to patching of the transporters on the surface (Figure 5B). This suggests that ABCB1a is closely associated/tethered to actin throughout its translocation cycle, consistent with the role of bundled actin in the stabilization of proteins on microvilli (Revenu *et al.*, 2011). Because the loss of actin bundle architecture also influences the localization of myosins (Revenu *et al.*, 2011), and given the aforementioned association between ABC transporters and myosins (Fu and Arias, 2012), myosin(s) could mediate tip localization of ABCB1 in sea urchins.

Why does ABCB1a localize to the tips of the microvilli? While the elongation of microvilli is an important mechanism for increasing the absorptive surface of cells, it may be a double-edged sword, coming at the cost of increasing uptake of toxicants. Positioning of transporters at or near microvillar tips could be a strategy to reduce the likelihood that effluxed molecules will be reabsorbed (Lange and Gartzke, 2001). This is consistent with models predicting that tip-effluxed molecules have a higher probability of escaping directly into the environment than those released along the shaft of the microvillus (Tran *et al.*, 2005; Acharya *et al.*, 2006). Moreover, estimates of the surface density of "efflux-active" (i.e., those transporters located at the microvillar tips) P-gp suggest that only 10% of the total P-gp in the cell, presumably a tip-localized fraction, contributes significantly to efflux (Tran *et al.*, 2005). The remainder likely resides in intracellular pools that can be recruited in response to stimuli (Kipp and Arias, 2002). Both the previous modeling results and our localization data support the finding that export of molecules is only achieved when sufficient efflux-active ABCB1a is at the microvillar tips.

Until recently, it had been presumed that microvilli are "passive" structures that simply increase cell surface area for absorption. However, selective targeting and precise positioning of membrane proteins along microvillar actin filaments in leukocytes (von Andrian *et al.*, 1995), macrophages, T-cells

(Singer *et al.*, 2001), and neuroepithelial cells (Weigmann *et al.*, 1997) and on both the enterocyte and renal brush border (McConnell *et al.*, 2009) suggest that actin-mediated segregation of microvillar membranes endows them with additional functions in cell defense, motility, and signaling. For example, in the enterocyte brush border, shedding of enzyme-rich microvillar tip membrane may protect the gut from infection by microbes (McConnell *et al.*, 2009). Our work highlights how microvillar tips are specialized regions of the membrane adapted for protection and underscores the importance of microvilli in cell physiology.

MATERIALS AND METHODS

Sea urchin collection and embryo culture

Adult *S. purpuratus* were collected in LaJolla, CA, and held in flow-through seawater aquaria at 10–12°C. Animals were injected with 0.55 M KCl to induce spawning. Eggs were washed twice with 0.22 µm filtered seawater (FSW), and sperm was collected undiluted. Eggs were dejellied for 3 min in FSW (adjusted to pH 4.8 with citric acid) and then washed twice in FSW. Eggs were diluted to 1000 eggs/ml in FSW containing 4 mM para-aminobenzoic acid and fertilized in a final dilution of 1:375,000 concentrated sperm. All batches achieved at least 95% fertilization. Fertilization envelopes were removed by passing the embryos twice through a 61-µm Nitex mesh. After the embryos had settled, excess sperm were removed by aspiration, and the embryos were resuspended in either calcium-free seawater or FSW and cultured at 13–15°C.

Phylogenetic analysis of ABCB1a

Recent studies have described the diversity and phylogenetic relationships of ABC transporters from the B family for various animals. Previously reported full transporters in the ABCB family for *Ciona intestinalis* (Annilo *et al.*, 2006), *Daphnia pulex* (Sturm *et al.*, 2009), *S. purpuratus* (Goldstone *et al.*, 2006), and sequences reported in these studies for *Drosophila melanogaster*, *Homo sapiens*, and *Saccharomyces cerevisiae* were downloaded. ABCB full transporters from the sea anemone *Nematostella vectensis* and the sponge *Amphimedon queenslandica* were identified by using human and *Drosophila* sequences in TBLASTN searches of genome assemblies and gene models for each species (*N. vectensis* version 1.0 at the Joint Genome Institute [Putnam *et al.*, 2007]; *A. queenslandica* at www.metazome.net/amphimedon [Srivastava *et al.*, 2010]). All ABCB sequences ($n = 25$) were aligned with MUSCLE (Edgar, 2004) and manually trimmed ($n = 1092$ characters).

Phylogenetic relationships for all proteins were determined using maximum likelihood (ML) and Bayesian analyses. ProtTest version 2.4 (Abascal *et al.*, 2005) was used to select the best model of protein evolution (model determined by Akaike's information criterion). The results indicated the best-fit model was LG + I + G + F, where I specifies a proportion of invariant sites, G specifies gamma-distributed rates across sites, and F specifies that empirical amino acid frequencies in the data set are used. ML analyses were conducted using RAxML version 7.2.6 (Stamatakis, 2006), and support for nodes was assessed with 1000 bootstraps. Bayesian analyses were performed with MrBayes version 3.2. MrBayes does not support the LG model for sequence evolution, so the second-best model from the ProtTest analysis (WAG + G + F) was used. Two independent analyses were performed with five chains run for five million generations, with trees sampled every 500 generations. The first 1.25 million generations were discarded as burn-in. Log likelihood values were plotted and found to be asymptotic well before the burn-in fraction. The Bayesian phylogeny is presented with posterior probability and ML bootstrap indicated for each branch (e.g., ML/Bayesian). Trees were visualized and illustrated with FigTree version 1.1.2 (http://tree.bio.ed.ac.uk/software/figtree). All trees were rooted with the ABCB transporter from *S. cerevisiae*.

Antibody generation and purification

Polyclonal antipeptide antibodies to *S. purpuratus* ABCB1a, (Ab1-C1 and Ab4-R2) were produced in chicken and rabbit, respectively, using the sequences representing amino acids 676–693 [KKEEEEEK-KENEVPLDDD] and amino acids 1304–1318 [EFGKHEELMAM-KQQY] of the ABCB1a cDNA clone (GenBank accession no. AAW28777; Hamdoun *et al.*, 2004). These peptide antibodies were custom-synthesized by two companies: Aves Lab (Tigard, OR) for Ab1-C1 and NEO BioScience (Cambridge, MA) for Ab4-R2. The antibodies were affinity-purified, resulting in immunoglobulin concentrations of 0.30 µg/µl (Ab1-C1) and 0.51 µg/µl (Ab4-R2).

To determine specificity of the purified antibodies for sea urchin ABCB1a, we tested antibodies adsorbed to immune peptides as negative controls (Figure S1) and used SF9 insect cell–expressed recombinant sea urchin ABCB1a as a positive control (Figure S1). For antibody competition experiments, both the rabbit (Ab4-R2) and chicken (Ab1-C1) antibodies were preincubated separately with 100× molar excess of Ab4-R2 and Ab1-C1 synthetic peptides at 12°C for 1.5 h. Preincubated peptide antibodies and untreated antibodies were then used for whole-mount immunolocalization as described in *Immunolocalization of ABCB1a*. Insect cell microsomes encoding recombinant sea urchin ABCB1a (GenBank accession no. NM001033950.1) were prepared by standard procedures (Evans *et al.*, 1995) and were provided as a generous gift by Solvo Biotechnology (Szeged, Hungary).

Western blots

Protein lysates of unfertilized *S. purpuratus* eggs and several PF stages (15 min, 45 min, 60 min, and 24 h PF) were prepared by lysing 5000 eggs or embryos in 150 µl of Fairbanks buffer (5 mM Tris-HCl, 1 mM EDTA, 5% sucrose, 1% SDS, 10 µg/ml pyronin Y, 40 mM dithiothreitol) containing 2X Complete, Mini protease inhibitor cocktail (Roche, Indianapolis, IN). Samples were heated to 55°C for 1 hr, and 15 µl (representing 500 eggs or embryos) were loaded onto a 7.5% SDS–PAGE gel. Following electrophoresis, proteins were transferred to nitrocellulose membrane and blocked in Tris-buffered saline (50 mM Tris, 150 mM NaCl, pH 7.4) containing 0.05% Tween 20 (TBST) and 5% nonfat dried milk overnight. Blots were then incubated for 3–4 h in blocking buffer containing either a 1:100 dilution of Ab4-R2 or 1:300 dilution of Ab1-C1 antibody. After three washes in TBST, blots were incubated for 1 h with the appropriate horseradish peroxidase (HRP)-conjugated secondary antibody diluted 1:5000 in blocking buffer and washed again in TBST. Detection of HRP activity on x-ray film was enhanced by SuperSignal West Pico Chemiluminescent Substrate kit (Thermo Scientific, Rockford, IL).

For Western blots of embryos overexpressing *S. purpuratus* ABCB1a, embryos were injected with mRNA encoding ABCB1a (GenBank accession no. NM001033950.1) as described in Shipp and Hamdoun (2012). The number of embryos loaded onto each lane was titrated to a level (80–100 embryos) at which amount the endogenous ABCB1a is not detectable by Western blots, but the overexpressed recombinant protein is readily detected. At the prehatch blastula stage (~18 h PF) embryos were harvested and prepared as described above. To determine the glycoforms of ABCB1a, we incubated protein-expressing embryos in 5 µM Bf-A or 10 µM cyclosporin A. Bf-A disrupts anterograde endoplasmic reticulum traffic to the Golgi, resulting in trapping of core proteins prior to

Golgi-mediated glycosylation (Loo and Clarke, 1997). Cyclosporin A induces hyperglycosylation of *S. purpuratus* ABCB1a.

Immunolocalization of ABCB1a

The optimum fixative for each stage was chosen based on retention of egg or embryo morphology with minimal shrinkage or swelling. Eggs and embryos were fixed for 30 min in 3.2% paraformaldehyde and 0.3% glutaraldehyde in either 100% phosphate-buffered saline (PBS; pH 8.0, for eggs and 15 min PF embryos), or 100% Millonig's PBS (MPBS; pH 7.0, for 45 and 60 min PF embryos), then incubated in antibody (1:10 for Ab1-C1 and 1:100 for Ab4-R2) diluted in 2% bovine serum albumin (BSA) in PBS/MPBS for 2 h; this was followed by a 1-h incubation in secondary antibody (Alexa Fluor 594–conjugated goat anti-chicken and goat anti-rabbit antibody; Life Technologies, Carlsbad, CA) diluted 1:500 in 2% BSA in PBS/MPBS. Samples were stained with 1 U/ml Alexa Fluor 488–phalloidin (Life Technologies) in PBS/MPBS for 15 min, before mounting in SlowFade Gold (Life Technologies) onto poly-L-lysine–coated MatTek dishes.

Each sample was divided between two MatTek dishes and imaged by confocal microscopy using a Zeiss LSM-700 laser-scanning confocal microscope (Jena, Germany) equipped with a Zeiss C-ApoChromat 63×/1.2 numerical aperture (NA) oil objective, and by 3D-SIM using a DeltaVision OMX 3D-SIM (Applied Precision, Issaquah, WA) microscope equipped with an Olympus 100×/1.4 NA oil objective and imaged with the 488- and 568-nm lasers using emission filters of 500–550 nm and 593–633 nm (512 × 512 pixels). 3D-SIM raw images were processed to reconstruct high-resolution information using Softworx version 5.0 software (Applied Precision).

Image analysis

Z-stacks of whole-mount embryos visualized by confocal microscopy were first deconvolved using Huygens Essential Software version 4.0 (Scientific Volume Imaging, Laapersveld, Netherlands). A theoretical point-spread function was used based on microscope parameters, model confocal parameters established by Huygens. and the Classic Maximum Likelihood Estimation algorithm to restore images. Sampling intervals were set manually to the actual experimental values, together with refractive indices and excitation/emission wavelengths.

Measurement of ABCB1a spots labeled with Alexa Fluor 594 and actin filaments labeled with Alexa Fluor 488, imaged by 3D-SIM, were performed using Imaris 7.3.1 software (Bitplane, Zurich, Switzerland). All 3D-SIM volume data were first processed to correct for illumination variations of scans of physical sections. Briefly, the mean and SD values of the intensity for an entire image Z-stack was computed using the Normalize Layer(s) function in Imaris. Then the mean and SD for all individual slices in the Z-stack were computed. Finally, the software adjusted the intensities of each Z-slice with a linear transformation to match the overall mean and SD value, and this procedure was applied to all Z-slices of the data set for each channel independently. Voxels with zero intensity were excluded from this calculation, as they were interpreted as background.

Three-dimensional surface reconstructions of actin filaments were rendered from the maximum intensity projection (MIP) to visualize the architecture of the microvillar network and to facilitate measuring the length of actin filaments. The Spots object tool in Imaris was used to render the ABCB1a protein spots in three dimensions and generate spot-associated statistics. For quantitative assessment of the three-dimensional distribution of ABCB1a protein in relation to the rendered actin filament, Z-stacks were further processed using the Imaris XT module, which integrates MATLAB applications (version 7.10; Mathworks, Natick, MA). A distance transformation function, in which the three-dimensional Euclidean distance was calculated from outside the closest actin surface reconstruction to the center of each voxel in the data set, was applied to the image, and the resultant distance was stored in a three-dimensional distance map. Overlaying the ABCB1a "spots" with this distance map allowed "spot" statistics to be generated and used to calculate the exact distance from the center of each overlaid "spot" to the closest actin surface. For ABCB1a spots within 200 nm of the actin surface, the distance of these spots from the tip of their associated microvilli was measured manually. Statistics for 10 microvilli and associated ABCB1a spots were measured for each of six eggs or embryos per time point (n = 6 embryos × 10 microvilli measured for each time point). Spot statistics were exported to Microsoft Office Excel software for analysis (Redmond, WA). MIP, spot, and surface renderings were assembled in Adobe Illustrator CS3 (San Jose, CA).

For analysis of ABCB1a distribution along F-actin microfilaments, cross-sectional images of eggs and embryos from 3D-SIM data were obtained in Imaris, imported into ImageJ (National Institutes of Health, Bethesda, MD), and used to measure six nonoverlapping intensity profiles of ABCB1a perpendicular to the cell surface. The intensity profiles were imported into Microsoft Office Excel for statistical analysis.

Effects of F-actin filament polymerization on ABCB1a translocation at fertilization

Embryos were exposed to 2 µM of cytochalasin D, latrunculin A, jasplakinolide, or dimethyl sulfoxide (DMSO) at 10 min and 50 min PF. At 60 min PF, embryos were fixed in 3.2% paraformaldehyde and 0.3% glutaraldehyde in MPBS for 30 min. Samples were processed through a series of primary (1:30 dilution of Ab1-C1) and secondary (1:500 dilution of Alexa Fluor 594–conjugated goat anti-chicken) antibodies as described above and imaged by confocal microscopy. See the Supplemental Material for details.

Effects of F-actin bundle formation on transport activation and ABCB1a localization

Intracellular changes in calcein accumulation in embryos activated with 30 µM of calcium ionophore A23187, grown in either FSW or NaFFSW, and exposed to 250 nM calcein-AM (acetoxymethyl ester) at 60 and 120 min postactivation for 1 h were imaged on the confocal microscope as described in the Supplemental Material. Additionally, a batch of ionophore-activated embryos grown in NaFFSW were exposed 40 mM NaCl at 60 min postactivation, exposed to 250 nM calcein-AM for 1 h at 120 min postactivation, and imaged by confocal microscopy. Immunolocalization of ABCB1a and actin in ionophore-activated embryos grown in NaFFSW was performed as described above and imaged by confocal microscopy. See the Supplemental Material for details.

Effects of Rab effector peptides on transporter activity

Effector domain peptides were custom-synthesized by Biomatik (Wilmington, DE): PEG-NHTIGVEFGSKIINAG (Rab4); PEG-ESTIGAAFLTQTVCLD (Rab5L); KATIGADFLTKEVMVD (Rab7); KSTIGVEFATRSIQVD (Rab11); and resuspended in deionized water at 5 mM. Unfertilized eggs were microinjected with peptides resuspended in deionized water at various concentrations and allowed to incubate for 45 min, and then fertilized with sperm (1:27,000) and incubated an additional 60 min. At 60 min PF, embryos were exposed to a final concentration of 250 nM calcein-AM for 90 min and imaged on the confocal microscope.

Immunolocalization of Rab11 with ABCB1a

The fixation of eggs and embryos was performed as described above. Samples were incubated for 2 h with the rabbit polyclonal anti-peptide Rab11 antibody, PA1-775 (Thermo Scientific, Waltham, MA) at 1:100 and Ab1-C1 at 1:150, and then labeled for 1 h with Alexa Fluor 594–conjugated goat anti-rabbit and Alexa Fluor 647–conjugated goat anti-chicken. Samples were stained with 1 U/ml Alexa Fluor 488–phalloidin in PBS/MPBS for 15 min, before being mounted in SlowFade Gold (Life Technologies) onto poly-L-lysine–coated MatTek dishes and visualized by confocal microscopy.

ACKNOWLEDGMENTS

We thank G. M. Moy, K. Uhlinger, K. Koda, and J. Roche for their experimental assistance and V. D. Vacquier for helpful discussions. We thank P. Zerofski for collection of research animals. Funding was provided by the National Institute of Child Health and Human Development (058070), the National Center for Research Resources (P30-NS047101), the Krinsk Research Advancement Initiative to A.H., a Scripps Postdoctoral Scholar Fellowship to K.W., and NICHD award 062178 to A.M.R.

REFERENCES

Abascal F, Zardoya R, Posada D (2005). ProtTest: selection of best-fit models of protein evolution. Bioinformatics 21, 2104–2105.

Acharya P, Tran TT, Polli JW, Ayrton A, Ellens H, Bentz J (2006). P-glycoprotein (P-gp) expressed in a confluent monolayer of hMDR1-MDCKII cells has more than one efflux pathway with cooperative binding sites. Biochemistry 45, 15505–15519.

Annilo T, Chen Z-Q, Shulenin S, Costantino J, Thomas L, Lou H, Stefanov S, Dean M (2006). Evolution of the vertebrate ABC gene family: analysis of gene birth and death. Genomics 88, 1–11.

Begg DA, Rebhun LI, Hyatt H (1982). Structural organization of actin in the sea urchin egg cortex: microvillar elongation in the absence of actin filament bundle formation. J Cell Biol 93, 24–32.

Bonder EM, Fishkind DJ, Cotran NM, Begg DA (1989). The cortical actin-membrane cytoskeleton of unfertilized sea urchin eggs: analysis of the spatial organization and relationship of filamentous actin, nonfilamentous actin, and egg spectrin. Dev Biol 134, 327–341.

Callaghan R, Crowley E, Potter S, Kerr ID (2008). P-glycoprotein: so many ways to turn it on. J Clin Pharmacol 48, 365–378.

Campanale JP, Hamdoun A (2012). Programmed reduction of ABC transporter activity in sea urchin germline progenitors. Development 139, 783–792.

Conner SD, Wessel GM (1998). rab3 mediates cortical granule exocytosis in the sea urchin egg. Dev Biol 203, 334–344.

Conner SD, Wessel GM (2000). A rab3 homolog in sea urchin functions in cell division. FASEB J 14, 1559–1566.

Dillon C, Goda Y (2005). The actin cytoskeleton: integrating form and function at the synapse. Annu Rev Neurosci 28, 25–55.

Edgar R (2004). MUSCLE: multiple sequence alignment with high accuracy and high throughput. Nucleic Acids Res 32, 1792–1797.

Epel D (1972). Activation of an Na^+-dependent amino acid transport system upon fertilization of sea urchin eggs. Exp Cell Res 72, 74–89.

Epel D (1975). The program of and mechanisms of fertilization in the echinoderm egg. Integr Comp Biol 15, 507–522.

Evans GL, Ni B, Hrycyna CA, Chen D, Ambudkar SV, Pastan I, Germann UA, Gottesman MM (1995). Heterologous expression systems for P-glycoprotein: *E. coli*, yeast, and baculovirus. J Bioenerg Biomembr 27, 43–52.

Fu D, Arias IM (2012). Intracellular trafficking of P-glycoprotein. Int J Biochem Cell Biol 44, 461–464.

Fu D, Roufogalis BD (2007). Actin disruption inhibits endosomal traffic of P-glycoprotein-EGFP and resistance to daunorubicin accumulation. Am J Physiol Cell Physiol 292, C1543-C1552.

Goldstone JV, Hamdoun A, Cole BJ, Howard-Ashby M, Nebert DW, Scally M, Dean M, Epel D, Hahn ME, Stegeman JJ (2006). The chemical defensome: environmental sensing and response genes in the *Strongylocentrotus purpuratus* genome. Dev Biol 300, 366–384.

Guggino WB, Stanton BA (2006). New insights into cystic fibrosis: molecular switches that regulate CFTR.. Nat Rev Mol Cell Biol 7, 426–436.

Hamdoun AM (2009). Reduced intracellular accumulation of calcein by overexpression of fluorescent protein fusions of the multidrug transporter *Sp*-ABCB1a, in sea urchin (*Strongylocentrotus purpuratus*) embryos. Mount Desert Island Biol Lab Bull 48, 59–62.

Hamdoun AM, Cherr GN, Roepke TA, Epel D (2004). Activation of multidrug efflux transporter activity at fertilization in sea urchin embryos (*Strongylocentrotus purpuratus*). Dev Biol 276, 452–462.

Kipp H, Arias IM (2002). Trafficking of canalicular ABC transporters in hepatocytes. Annu Rev Physiol 64, 595–608.

Lange K, Gartzke J (2001). Microvillar cell surface as a natural defense system against xenobiotics: a new interpretation of multidrug resistance. Am J Physiol Cell Physiol 281, C369–C385.

Loo TW, Clarke DM (1997). Correction of defective protein kinesis of human p-glycoprotein mutants by substrates and modulators. J Biol Chem 272, 709–712.

Loo TW, Clarke DM (2008). Mutational analysis of ABC proteins. Arch Biochem Biophys 476, 51–64.

McConnell RE, Higginbotham JN, Shifrin DA, Jr., Tabb DL, Coffey RJ, Tyska M (2009). The enterocyte microvillus is a vesicle-generating organelle. J Cell Biol 185, 1285–1298.

Nicolaou M, Andress EJ, Zolnerciks JK, Dixon PH, Williamson C, Linton KJ (2011). Canalicular ABC transporters and liver disease. J Pathol 226, 300–315.

Otto JJ, Kane RE, Bryan J (1980). Redistribution of actin and fascin in sea urchin eggs after fertilization. Cell Motil 1, 31–40.

Polyak K, Weinberg RA (2009). Transitions between epithelial and mesenchymal states: acquisition of malignant and stem cell traits. Nat Rev Cancer 9, 265–273.

Putnam NH *et al.* (2007). Sea anemone genome reveals ancestral eumetazoan gene repertoire and genomic organization. Science 317, 86–94.

Revenu C *et al.* (2011). A new role for the architecture of the microvillar actin bundles in apical retention of membrane proteins. Mol Biol Cell 23, 324–336.

Schroeder TE (1979). Surface area change at fertilization: resorption of the mosaic membrane. Dev Biol 70, 306–326.

Schroeder TE (1988). Contact-independent polarization of the cell surface and cortex of free sea urchin blastomeres. Dev Biol 125, 255–264.

Shi Z *et al.* (2009). Inhibiting the function of ABCB1 and ABCG2 by the EGFR tyrosine kinase inhibitor AG1478. Biochem Pharmacol 77, 781–793.

Shipp LE, Hamdoun A (2012). ATP-binding cassette (ABC) transporter expression and localization in sea urchin development. Dev Dyn 241, 1111–1124.

Singer II *et al.* (2001). CCR5, CXCR4, and CD4 are clustered and closely apposed on microvilli of human macrophages and T cells. J Virol 75, 3779–3790.

Spudich A, Spudich JA (1979). Actin in triton-treated cortical preparations of unfertilized and fertilized sea urchin eggs. J Cell Biol 82, 212–226.

Spudich A, Wrenn JT, Wessells NK (1988). Unfertilized sea urchin eggs contain a discrete cortical shell of actin that is subdivided into two organizational states. Cell Motil Cytoskeleton 9, 85–96.

Srivastava M *et al.* (2010). The *Amphimedon queenslandica* genome and the evolution of animal complexity. Nature 466, 720–726.

Stamatakis A (2006). Maximum likelihood-based phylogenetic analyses with thousands of taxa and mixed models. Bioinformatics 22, 2688–2690.

Sturm A, Cunningham P, Dean M (2009). The ABC transporter gene family of *Daphnia pulex*. BMC Genomics 10, 170.

Tran TT, Mittal A, Aldinger T, Polli JW, Ayrton A, Ellens H, Bentz J (2005). The elementary mass action rate constants of P-gp transport for a confluent monolayer of MDCKII-hMDR1 cells. Biophys J 88, 715–738.

Vacquier VD (1981). Dynamic changes of the egg cortex. Dev Biol 84, 1–26.

von Andrian UH, Hasslen SR, Nelson RD, Erlandsen SL, Butcher EC (1995). A central role for microvillous receptor presentation in leukocyte adhesion under flow. Cell 82, 989–999.

Wakabayashi Y, Dutt P, Lippincott-Schwartz J, Arias IM (2005). Rab11a and myosin Vb are required for bile canalicular formation in WIF-B9 cells. Proc Natl Acad Sci USA 102, 15087–15092.

Wang L, Soroka CJ, Boyer JL (2002). The role of bile salt export pump mutations in progressive familial intrahepatic cholestasis type II. J Clin Invest 110, 965–972.

Weigmann A, Corbeil D, Hellwig A, Huttner WB (1997). Prominin, a novel microvilli-specific polytopic membrane protein of the apical surface of epithelial cells, is targeted to plasmalemmal protrusions of non-epithelial cells. Proc Natl Acad Sci USA 94, 12425–12430.